Synthesis, characterization, and application of ZnO/TiO$_2$ nanocomposite for photocatalysis of a herbicide (Bentazon)

Mitra Gholami[a], Mehdi Shirzad-Siboni[a,*], Mahdi Farzadkia[a], Jae-Kyu Yang[b]

[a]*Department of Environmental Health Engineering, School of Public Health, Iran University of Medical Sciences, Tehran, Iran,
Tel. +98 9123906308; emails: gholamimitra32@gmail.com, gholamim@iums.ac.ir (M. Gholami), Tel. +98 9112346428;
Fax: +98 2188607939; emails: mshirzadsiboni@yahoo.com, shirzad.m@iums.ac.ir (M. Shirzad-Siboni), Tel. +98 9122588677;
email: mahdifarzadkia@gmail.com (M. Farzadkia)*
[b]*Division of General Education, Kwangwoon University, Seoul, Republic of Korea, Tel. +82 2 940 5769; email: jkyang@kw.ac.kr*

ABSTRACT

The purpose of this investigation was to study the applicability of ZnO–TiO$_2$ composite as a photocatalyst for degradation of Bentazon. Effects of various parameters such as catalyst dosage, pH, initial Bentazon concentration, oxygen purging gas, hydrogen peroxide concentration and type of organic compounds on the removal efficiency of Bentazon were studied. The results of SEM and FT-IR analysis demonstrated favorable immobilization of zinc oxide nanoparticles onto TiO$_2$. The greatest removal of Bentazon was observed at neutral pH due to photo-corrosion of ZnO on composite in acidic and basic conditions. The pseudo-first-order rate constant (k_{obs}) and electrical energy per order (E_{Eo}) were greatly dependent on the Bentazon concentration. Removal efficiency of Bentazon was increased with O$_2$ purging and addition of H$_2$O$_2$, while it was decreased in the presence of organic compounds. Removal efficiency of Bentazon by UV/ZnO/TiO$_2$ process was greater than that by UV/TiO$_2$ process, UV/ZnO, and UV alone. Photocatalytic activity was maintained even after five successive cycles.

Keywords: Photocatalysis; Bentazon; Nanocomposite; Zinc oxide/titanium oxide

1. Introduction

Major sources of herbicide contamination in surface and groundwater are chemical spills, industrial effluents, agricultural runoffs, and leaching [1]. Bentazon, also known as Basagran by the trade name, is a selective post-emergence herbicide used to control many broadleaf weeds and sedges primarily by contact action in most gramineous and many large seeded leguminous crops such as food and feed crops including alfalfa, beans, corn, peanuts, peas, asparagus, cereals, peppers, peppermint, rice, and sorghum [2–5]. Due to its persistence, stability and toxicity in the environment, it causes much concern to regulation authorities and environmental protection societies. It is harmful to human when it is swallowed or absorbed through the skin and sometimes causes irritation to the eyes [2]. Thus, it is classified as toxicity class III, slightly toxic, and dangerous for the environment. The maximum permissible concentration of Bentazon in drinking water is known as 0.03 mg/L [6]. Therefore, surface and groundwater contaminated with persistent herbicide such as Bentazon should be treated with suitable physicochemical and/or

*Corresponding author.

biological treatment processes. Advanced oxidation processes are one of the plausible treatment processes and have much attention to overcome these problems [3,7–10]. Among several semiconductors, ZnO and TiO$_2$ have been proven to be promising photocatalysts due to their intriguing optical and electric properties, low cost, stability, nontoxicity, and ease of availability [11–13]. Compared with single ZnO or TiO$_2$, their composite has a superior photocatalytic activity owing to the extension of light absorption range and effective charge transfer from ZnO to TiO$_2$ [14]. Photocatalysis using hybrid semiconductors is a novel approach to achieve a more efficient charge separation, an increased lifetime of the charge carriers, and an enhanced interfacial charge transfer to adsorbed substrates [15,16]. Several nanocomposites such as TiO$_2$–poly(vinylidenefluoride) [16], TiO$_2$-graphene [15], nanosized zinc oxide [17], Ca–Ce–W–TiO$_2$ [11], Fe$_3$O$_4$/hydroxyapatite [18], ZnS/TiO$_2$ [19], and TiO$_2$/H-MOR [20] have been applied in the removal of pesticides and herbicides. Also there are many reports about photocatalytic degradation of Bentazon with TiO$_2$ or ZnO [4,8,21]. However, only limited information is available for the removal efficiency and removal kinetics of Bentazon with illuminated ZnO/TiO$_2$ nanocomposite.

Therefore, this study examined the degradation of Bentazon in aqueous solution by ZnO/TiO$_2$ nanocomposite under UV-C (247.3 nm) irradiation. The effect of photocatalyst dosage, initial pH, and initial Bentazon concentration, type of purging gas, hydrogen peroxide concentration, and type of organic compounds on the photocatalytic degradation of Bentazon was investigated. Additionally, kinetic study was conducted by the application of zero, first, second, and Langmuir–Hinshelwood kinetic model. The electrical energy per order (E_{Eo}) was calculated to evaluate cost-efficiency of the processes.

2. Materials and methods

2.1. Chemicals

Zinc chloride (99.5%), sodium hydroxide, organic compounds, and hydrochloric acid were purchased from Merck Company (Germany) and used without any purification. P-25 TiO$_2$ (80/20 mixture of anatase and rutile) was obtained from Degussa Corp. It had approximately spherical shape and had greater than 99.5% purity. The specific surface area of the TiO$_2$ particles was 50 ± 15 m^2/g according to Evonik-Industrial Co. The average size of the TiO$_2$ particles was 21 nm. The herbicide Bentazon was purchased from Chemservice (USA). Its chemical structure and other

characteristics are listed in Table 1 [22]. The experimental reactor used for the photocatalytic degradation of Bentazon is shown in Fig. 1. A 125 W medium-pressure UVC lamp (Arda, France) emitting maximum wavelength at 247.3 nm (1,020 μw/cm^2) was applied as a light source.

2.2. Preparation of ZnO/TiO$_2$ nanocomposite

TiO$_2$ was dried at 103°C for 3 h in an oven. ZnCl$_2$ and NaOH was used as a starting agent and as a precipitant, respectively. ZnO nanoparticles were synthesized adopting the method that reported in the previous work [23]. A stock solution (pH 6) of 0.1 mol/L zinc chloride (ZnCl$_2$) was prepared by dissolution of zinc chloride into distilled water. Then an alkaline stock solution (pH 13.3) of 0.2 M NaOH was prepared in deionized water. TiO$_2$ was added to the ZnCl$_2$ solution at the ratio of 1:1 (w/w). Sodium hydroxide solution was added dropwise to the precursor solution to obtain an alkaline medium (pH 12) producing a white, gelatinous ZnO/TiO$_2$ product. The synthetic reaction was fundamentally performed for 7 h with stirring. The products in aqueous solution were centrifuged (Sigma-301, 4000 rpm, Germany), washed with deionized water, and then dried at 100°C for 3 h [14]. Field emission scanning electron microscopy (FE-SEM, MIRA3, Tescan, Czech Republic), energy dispersive X-ray spectroscopy (EDX, TESCA MIRA3, Czech Republic), X-ray diffraction (XRD, D8 Advance, Bruker, Germany), and Fourier transform infrared spectroscopy (FT-IR, Tensor 27, Bruker, Germany) techniques were used for characterization of the prepared ZnO/TiO$_2$ nanocomposite. The pH$_{\text{ZPC}}$

Table 1
Structure and characteristics of Bentazon

Structure

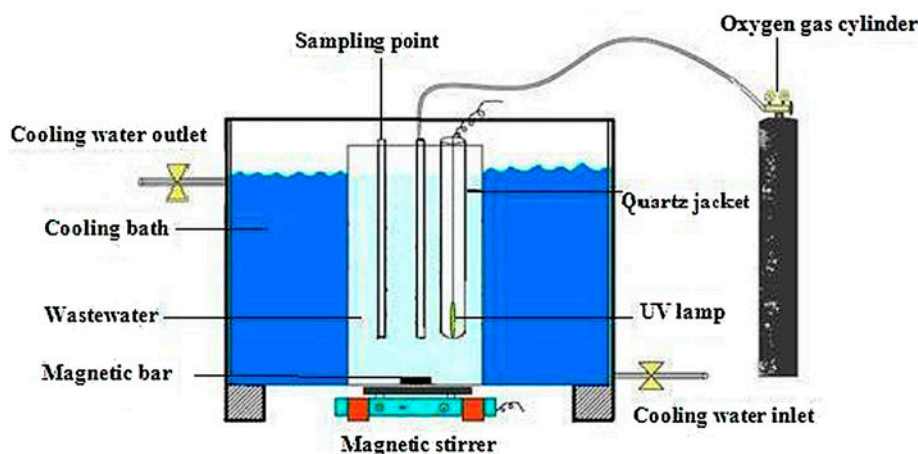| Formula	C$_{10}$H$_{12}$N$_2$O$_3$S
$\lambda_{\max}$ (nm)	335
M_{w} (g/mol)	240.3
Solubility in water (g/L)	0.50
pK_{a} (24°)	3.3
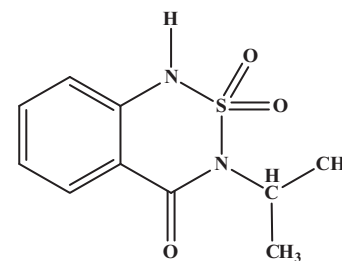
Fig. 1. A schematic flow diagram of the experimental reactor.

of ZnO/TiO$_2$ nanocomposite was determined adopting the method previously reported [24–27].

2.3. Experimental procedure and analysis

Stock solution (1,000 ppm) of Bentazon was prepared by dissolving Bentazon into distilled water. In each experiment, a certain dosage of nanocatalyst (0.25–2 g/L) was poured in 1 L of Bentazon solution with a distinct concentration (5–50 mg/L) at a certain pH (3–11). The initial pH of solution was adjusted by adding NaOH or HCl(0.1 M) and measured by pH meter (Metron, Switzerland). All runs were performed under ambient conditions for 2 h. The solution in the photo-reactor was kept at constant temperature (25 ± 1°C) and constantly stirred. The solution loaded with nanocatalyst was equilibrated in the dark for 30 min. After the equilibration period, the UV-lamp was switched on and 10 mL of solution was taken at definite time intervals. The aqueous sample was centrifuged (Sigma-301, Germany) at 4,000 revolution per minute (rpm) for 10 min to eliminate nanocatalyst and then residual Bentazon concentration in the suspension was analyzed. The concentration of the Bentazon in each sample was measured using a spectrophotometer (UV/vis spectrophotometer, Hach-DR 5000, USA) at λ_{max} = 335 nm by a calibration curve based on Beer–Lambert law [28].

3. Results and discussion

3.1. Characterization of nanocomposite

3.1.1. XRD analysis

The XRD patterns of TiO$_2$, ZnO, and ZnO/TiO$_2$ composite are illustrated in Fig. 2. The patterns exhibit crystalline structure of both ZnO and TiO$_2$ even after the immobilization of ZnO on TiO$_2$. The main peaks at 2θ values of 31.92, 34.6, and 36.48 correspond to the (1 0 0), (0 0 2), and (1 0 1) planes of hexagonal wurtzite ZnO (JCPDS card No. 36-1451). As illustrated in Fig. 2, after immobilization of ZnO, the peaks related to the ZnO are still observed, which indicates the growth of the ZnO crystal on the TiO$_2$ particles. The mean crystallite size of the ZnO/TiO$_2$ composite was estimated to be about 10 nm using the Debye–Sherrer's equation.

3.1.2. FT-IR analysis

The functional groups on the surface of photocatalyst can play a significant role in the photocatalytic activity because photocatalytic reactions mostly occur on the surface of photocatalyst. Thus, FT-IR analyses of ZnO, TiO$_2$, and ZnO/TiO$_2$ composite were performed in the range of 400–4,000 cm^{-1} (Fig. 3). FT-IR spectrum of the synthesized ZnO nanorods showed significant absorption peaks at 458, 727, 913, and 3,500 cm^{-1}. The band observed between 400 and 500 cm^{-1} can be corresponding to stretching vibration of ZnO. The weak band near 1,590 cm^{-1} is assigned to H–O–H bending vibration mode due to the adsorption of moisture when FT-IR sample disks were prepared in an open air atmosphere [29]. The band at 3,500 cm^{-1} is corresponding to the presence of hydroxyl groups ($^-$OH). As shown in Fig. 3, the band located at 481 cm^{-1} can be attributed to ZnO which is observable on the spectrum of both pure ZnO and its immobilized form. For the case of TiO$_2$ nanoparticles, the peak at 438 and 620 cm^{-1} is attributed to the E$_g$ and A$_{2g}$ mode, respectively [30]. The results of FT-IR analysis proved the hybridization of ZnO nanorods with TiO$_2$.
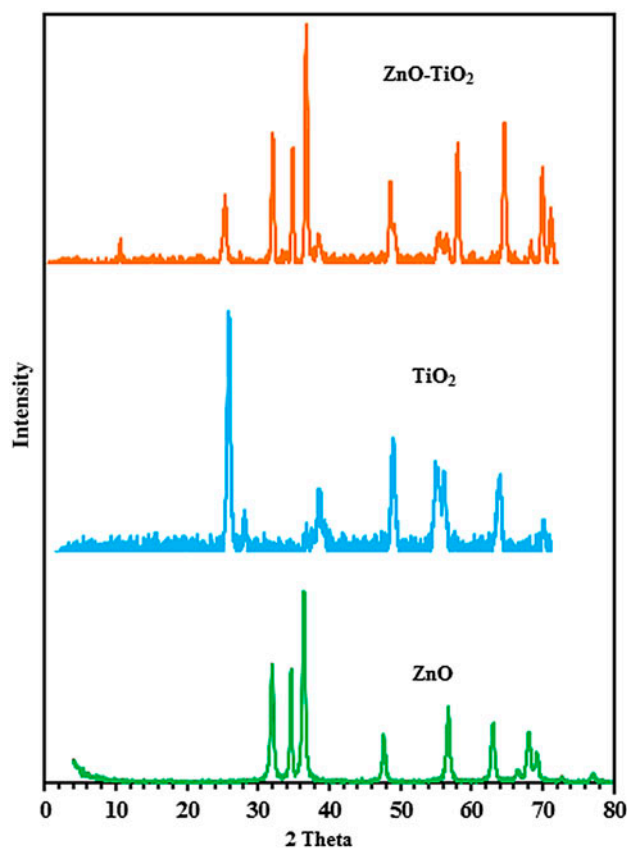
Fig. 2. Typical XRD patterns of samples.

Fig 3. FT-IR spectra of samples.

3.1.3. SEM and EDX analysis

FE-SEM was carried out by a Mira microscope to obtain the surface morphology of ZnO nanoparticles and ZnO/TiO$_2$ nanocomposite using an EDX. SEM images of ZnO nanoparticles and ZnO/TiO$_2$ nanocomposite are shown in Fig. 4(a) and (b), respectively. As shown in Fig. 4(b), ZnO/TiO$_2$ nanocomposite was composed of TiO$_2$ nanoparticles and ZnO nanorods. EDX microanalysis was used to characterize the elemental composition of the ZnO/TiO$_2$ nanocomposite. EDX pattern of the ZnO nanoparticles and ZnO/TiO$_2$ nanocomposite is depicted in Fig. 5(a) and (b), respectively. According to the results of EDX analysis, the major elements were Zn (31.54%), O (14.44%), and Ti (7.32%), indicating good hybridization between ZnO and TiO$_2$.

3.2. Effects of operational parameters

3.2.1. Effect of catalyst dosage

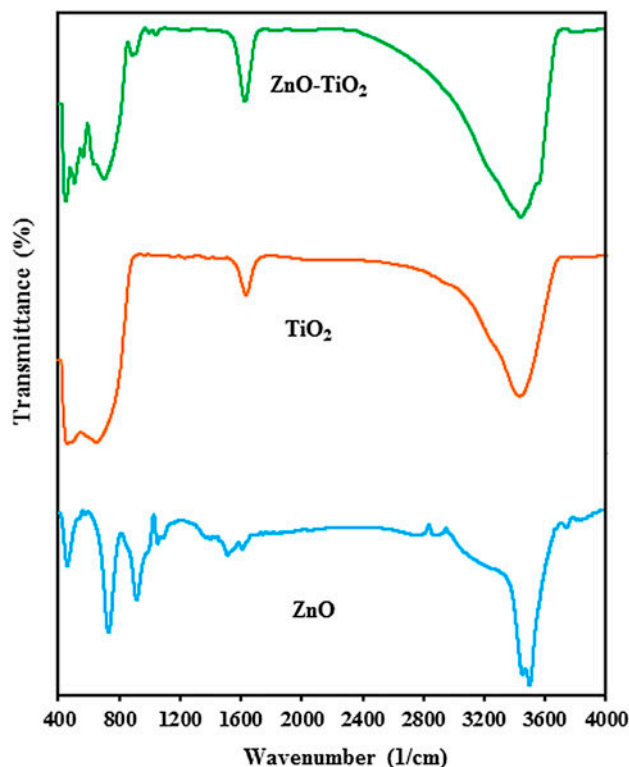Effect of catalyst dosage on the degradation of Bentazon by UV/ZnO/TiO$_2$ process was investigated by varying the catalyst dosage (0.25, 0.5, 1, 2 g/L) at initial pH 7 and initial Bentazon concentration (20 ppm) for different time interval. Fig. 6 shows the degradation efficiency enhanced from 64.4 to 84.2% by increasing the catalyst dosage from 0.25 to 5 g/L and then decreased to 69.3% in catalyst dosage equal to 2 g/L. Without UV irradiation, the degradation efficiency varied from 1.7 to 20.5% depending on the photocatalyst dosage due to the adsorption of Bentazon. The most effective decomposition of Bentazon was observed at 0.5 g/L of nanocatalyst (84.2%), which was chosen as optimum amount. Total active surface area can be enhanced with increasing photocatalyst dosage from 0.25 to 0.5 g/L, causing increased degradation of Bentazon. But, further increase in ZnO/TiO$_2$ concentration above 0.5 g/L resulted in lower degradation of Bentazon. This may be due to the aggregation of ZnO/TiO$_2$ under high particle concentration which reduces the interfacial area between the reaction mixture and the photocatalyst, reducing light penetration. This result agrees well with previous studies for the degradation of herbicides [8,21]. Based on the results, an optimum ZnO/TiO$_2$ dosage for degradation of the Bentazon in aqueous solution was determined as 0.5 g/L.
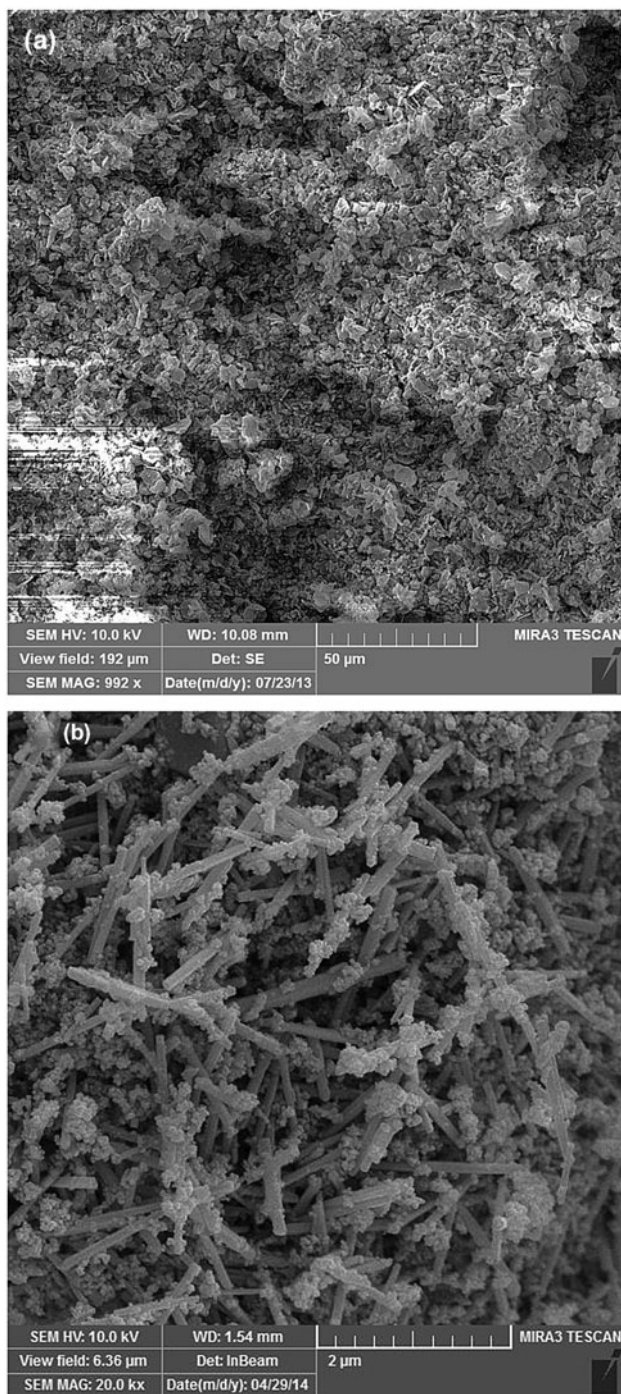
Fig. 4. SEM image of samples (a) ZnO nanoparticles and (b) ZnO/TiO$_2$ nanocomposite.

Fig. 5. EDX image of samples (a) ZnO nanoparticles and (b) ZnO/TiO$_2$ nanocomposite.

Fig. 6. The effect of catalyst dosage on the photocatalytic degradation of Bentazon (pH 7, [Bentazon]$_0$ = 20 ppm).

3.2.2. Effect of initial pH

Effect of initial pH on the degradation of Bentazon by UV/ZnO/TiO$_2$ process was investigated by varying the initial pH from 3 to 11 at initial Bentazon concentration (20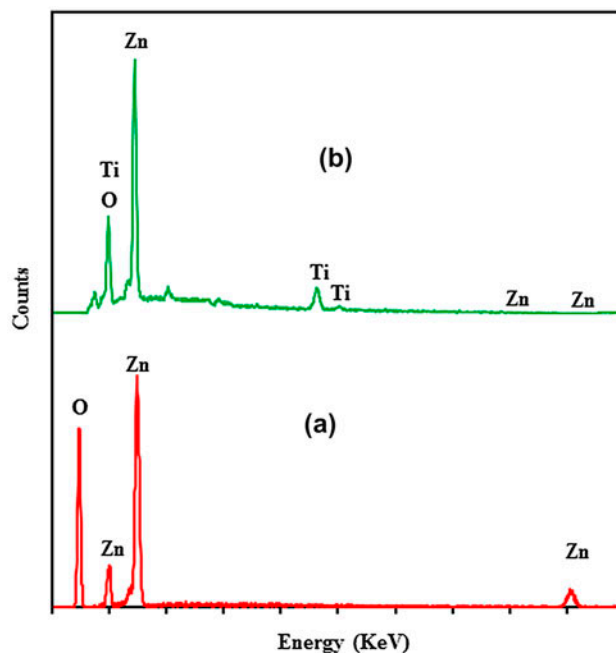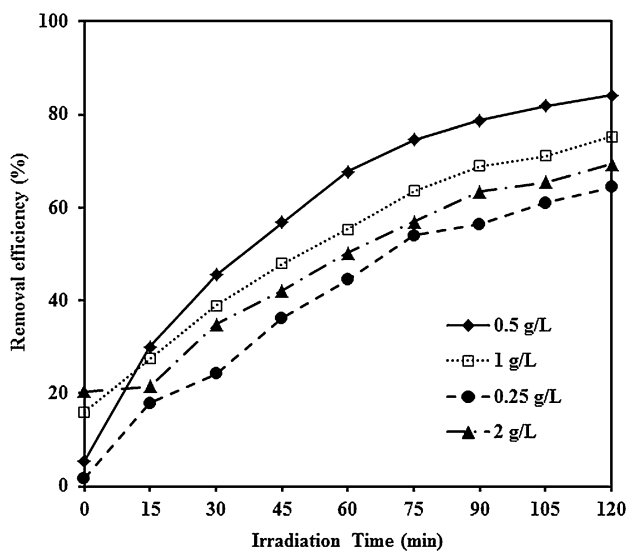 ppm) and catalyst dosage of 0.5 g/L for different time interval. Fig. 7 shows the effect of initial pH on the degradation of Bentazon. Fig. 7 shows that the degradation efficiency enhanced from 45.43 to 84.2% by increasing the initial pH from 3 to 7 and then decreased to 19.8% in pH equal to 11. In our previous work, the pH$_{pzc}$ of ZnO/TiO$_2$ nanocomposite was about 6 [14]. The pH$_{pzc}$ of ZnO is known as 9,

from previous studies [31]. The ZnO/TiO$_2$ nanocomposite surface will be positively charged in acidic medium (pH < 6) as described in Eq. (1), whereas it will be negatively charged in alkaline medium (pH > 6) as described in Eq. (2). Also, stability of ZnO–TiO$_2$ nanocomposite has been assessed at different solution pH values. According to the pH$_{pzc}$ data, the results showed that ZnO–TiO$_2$ nanocomposite is stable in acidic solutions (pH > 2).

$$\begin{aligned} \mathrm{pH} < \mathrm{pH}_{PZC} : {} & > \mathrm{Ti-OH \ or} > \mathrm{Zn-OH} + \mathrm{H}^+ \\ & \leftrightarrow \ > \mathrm{Ti-OH_2^+ \ or} > \mathrm{Zn-OH_2^+} \end{aligned} \quad (1)$$

$$\begin{aligned} \mathrm{pH} > \mathrm{pH}_{PZC} : {} & > \mathrm{Ti-OH \ or} > \mathrm{Zn-OH} + \mathrm{OH}^- \\ & \leftrightarrow \ > \mathrm{Ti-O^- \ or} > \mathrm{Zn-O^-} + \mathrm{H_2O} \end{aligned} \quad (2)$$
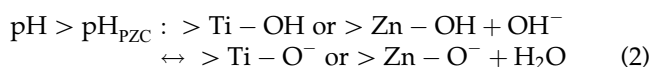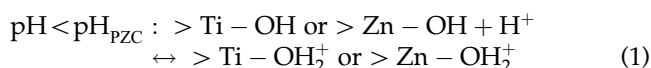
Effect of pH on the photocatalytic activity can be explained by electrostatic interaction between the catalyst surface and the target compound, chemical stability of ZnO–TiO$_2$ in addition to variation of redox potential of photocatalyst at different pH. The given pK_a for Bentazon is 3.3 [3,21]. Only considering electrostatic interaction, an optimal condition is regarded as p$K_a^{\mathrm{Bentazon}} < \mathrm{pH} < \mathrm{pH}^{\mathrm{ZnO-TiO_2}}_{PZC}$ at which the positively charged ZnO/TiO$_2$ and negatively charged Bentazon should readily attract each other. The increased degradation with increasing pH from 3 to 7 may be attributed to an efficient adsorption of substrate on the catalyst surface due to attraction between positively charged ZnO–TiO$_2$ nanocomposite surface

and negatively charged Bentazon molecules. However, ZnO becomes unstable at low and at high pH [4,8,21]. Generally photocatalysts have greater redox potential at low pH. Therefore, the greatest removal of Bentazon observed at pH 7 can be explained by combined effect of different trend of adsorption, chemical stability of ZnO–TiO$_2$ in addition to variation of redox potential of photocatalyst at different pH. From this study, pH 7 was identified as an optimum condition for the removal of Bentazon using ZnO/TiO$_2$ nanocomposite.

3.2.3. Effect of initial Bentazon concentration

Effect of initial Bentazon concentration on the degradation of Bentazon by UV/ZnO/TiO$_2$ process was investigated with variation of initial Bentazon concentration (5, 10, 20, 30, 40, 50 ppm) at initial pH 7 and at constant catalyst dosage (0.5 g/L) for different time interval. Fig. 8 shows the effect of initial Bentazon concentration on the degradation of Bentazon. Fig. 8 shows that the photocatalytic degradation of Bentazon was decreased from 99.9 to 29.1% with increasing the initial Bentazon concentration from 5 to 50 ppm after 2 h. The presumed reason is that when the concentration of Bentazon increased, adsorbed fraction of Bentazon on the surface of ZnO/TiO$_2$ nanocomposite increased. The large amount of adsorbed Bentazon can cause inhibitive effect on the reaction of Bentazon molecules with photogenerated holes or hydroxyl radicals because of the lack of any direct contact between them. As the concentration of herbicide increase, it also absorbs much fraction of light, causing little utilization of photons by the photocatalyst surface [11,31]. Similar results have been reported by other researchers [1,7,32–36].

3.2.4. Kinetics and electrical energy per order (E$_{Eo}$) studies

This section will deal with finding the suitable chemical degradation model that can describe the experimental kinetic data. In order to obtain the kinetic information, the experimental results were fitted with zero, first- and second-order equations (Eqs. (3–5)) [31,37–40]:
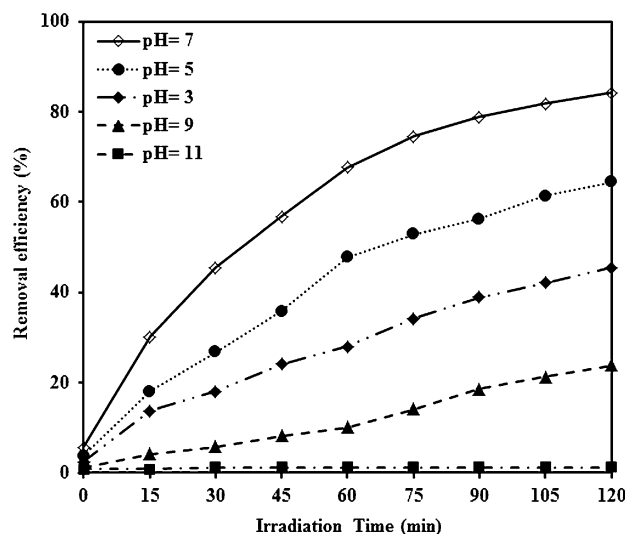
$$C_0 - C_t = k_0 t \quad (3)$$

Fig. 7. The effect of initial pH on the photocatalytic degradation of Bentazon (catalyst dosage = 0.5 g/L, [Bentazon]$_0$ = 20 ppm).

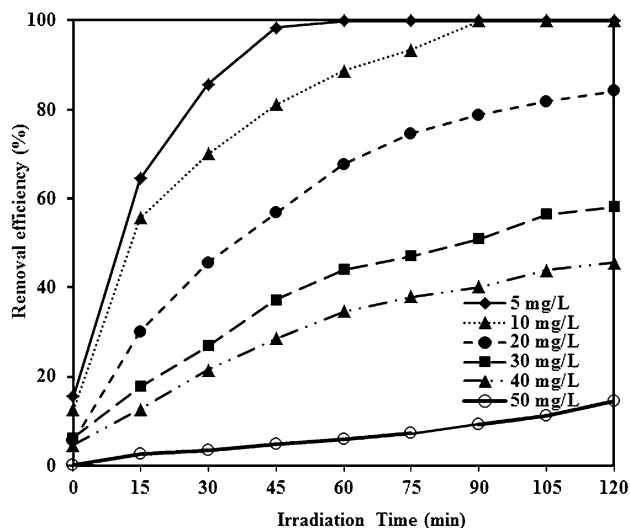$$\ln \frac{C_0}{C_t} = k_{\mathrm{obs}} \, t \quad (4)$$

Fig. 8. The effect of initial Bentazon concentration on the photocatalytic degradation of Bentazon (catalyst dosage = 0.5 g/L, pH 7).

$$\frac{1}{C_0} - \frac{1}{C_t} = k_2 t \tag{5}$$

where C_0 and C_t are the concentration of Bentazon (ppm) at initial and time t, respectively. k_0 (mol/L/min), k_{obs} (min^{-1}), and k_2 (L/mol/min) are the zero-, first-, and second-order rate constants, respectively. To obtain the kinetic data of the photocatalytic degradation of Bentazon, $C_0 - C_t$, ln[C_0/C] and $\frac{1}{C_0} - \frac{1}{C_t}$ vs. t was plotted. The zero, first, and second kinetic parameters for the photocatalytic degradation of Bentazon at different initial Bentazon concentrations are given in Table 2. The kinetic data for photocatalytic degradation of Bentazon showed the best fitting with the first-order model. As can be seen from Table 2, the pseudo-first-order rate constant (k_{obs}) and R^2 were decreased from 0.0649 to 0.0032 min^{-1} and 0.9987–0.9315 with increasing the initial Bentazon concentration from 5 to 50 ppm, respectively. The relationship between initial degradation rate (r) and initial concentration of Bentazon for a heterogeneous photocatalytic degradation process can be described by Langmuir–Hinshelwood model (Eqs. (6 and 7)) [4,31,37]:

$$-\frac{d[\text{Bentazon}]}{dt} = \frac{k_c K_{\text{Bentazon}}[\text{Bentazon}]}{1 + K_{\text{Bentazon}}[\text{Bentazon}]_0}$$
$$= k_{obs}[\text{Bentazon}] \tag{6}$$

$$\frac{1}{k_{obs}} = \frac{1}{k_c K_{\text{Bentazon}}} + \frac{[\text{Bentazon}]_0}{k_c} \tag{7}$$

where [Bentazon]$_0$ is the initial concentration of Bentazon in ppm, k_c (mg/L/min) is the kinetic rate constant of surface reaction, and K$_{\text{Bentazon}}$ (L/mg) is the Langmuir adsorption constant.

Therefore, k_{obs} values for each initial concentration (Table 2) were found from the slope of straight line of ln ([Bentazon]$_0$/[Bentazon]) vs. reaction time plot. The values of K$_{\text{Bentazon}}$ and k_c were calculated as 0.162 (L/mg) and 0.154 (mg/L/min) by plotting $1/k_{obs}$ vs. initial Bentazon concentration, respectively. Pourata et al. [4] reported a Langmuir–Hinshelwood equation constant of 0.0517 (mg/L/min) for the photocatalytic degradation of Bentazon(15 ppm) in the presence of synthesized nanocrystalline TiO$_2$ powders as a photocatalyst [4]. Devipriy and Yesodharan [32] reported a Langmuir–Hinshelwood equation constant of 0.075 (mg/L/min) for the photocatalytic degradation of Bentazon (0.1325 mM) with solar/TiO$_2$ [32].

The zero, first, and second kinetic parameters for the photocatalytic degradation of Bentazon at different pHs are given in Table 3. Photocatalytic degradation of Bentazon at different pHs was better fitted with the second-order model than the zero- and first-order model.

Considering the economic point of view, E_{Eo} of the photocatalytic degradation of Bentazon, defined as the number of kWh of electrical energy required to reduce the concentration of a pollutant by one order of magnitude (90%) in 1 m^3 of contaminated water, was applied to evaluate cost-efficiency of the process. The E_{Eo} (kWh/m^3) can be calculated via Eq. (8) [4,31]:

$$E_{EO} = \frac{38.4 \times P}{V \times k_{obs}} \tag{8}$$

$$E_{EO} = \frac{p \times t \times 1000}{V \times 60 \times \log(C_i/C_f)} \tag{9}$$

where P is the rated power (kW) of the process, k_{obs} is the pseudo-first-order rate constant (min^{-1}), and V is the volume (L) of the solution in the reactor. E_{Eo} of the process at different initial Bentazon concentration are summarized in Table 2. Table 2 presents that E_{EO} value was increased from 73.96 to 1,500 (kWh/m^3) with increasing initial Bentazon concentration from 5 to 50 ppm. Also electrical energy per order (E_{Eo}) for any process is calculated. The result presents that the E_{EO} value for UV/ZnO/TiO$_2$ (312.19) process is lower than that for UV/TiO$_2$ (550.04), UV/ZnO (1418.84), and UV (14101.38) process.

Table 2
Kinetic parameters for the photocatalytic degradation of Bentazon at different initial concentrations (catalyst dosage = 0.5 g/L and pH 7)

| [Bentazon]$_0$ (ppm) | Zero-order | | k_{obs} (min^{-1}) | First-order | | E_{Eo} (kWh/m^3) | Second-order | |
	k_0 (mol L^{-1} min^{-1})	R^2		$1/k_{obs}$ (min)	R^2		k_2 (L mol^{-1} min^{-1})	R^2
5	0.0298	0.5384	0.0649	15.4	0.9987	73.96	0.2473	0.6808
10	0.0673	0.7234	0.0346	28.9	0.9903	138.73	0.0125	0.9343
20	0.1281	0.8712	0.0154	64.9	0.9844	311.69	0.0022	0.9807
30	0.1435	0.916	0.0071	140.84	0.9697	676.06	0.0004	0.9939
40	0.135	0.9155	0.0049	204.08	0.9557	979.59	0.0002	0.9825
50	0.108	0.9694	0.0032	312.5	0.9315	1,500	0.0001	0.9315

Table 3
Kinetic parameters for the photocatalytic degradation of Bentazon at different initial pH ([Bentazon]$_0$ = 20 ppm, catalyst dosage = 0.5 g/L)

| pH | Zero-order | | First-order | | Second-order | |
	k_0 (mol L^{-1} min^{-1})	R^2	k_1 (min^{-1})	R^2	k_2 (L mol^{-1} min^{-1})	R^2
3	0.0709	0.9645	0.0009	0.9873	0.0003	0.9948
5	0.1031	0.9394	0.005	0.9861	0.0008	0.9942
7	0.1281	0.8712	0.0154	0.9844	0.0023	0.9848
9	0.0395	0.9881	0.0022	0.9766	0.0001	0.9755
11	0.0014	0.4807	0.0001	0.5299	0.0001	0.4875

3.2.5. Effect of purging of oxygen gas

Effect of purging of oxygen gas and variation of DO concentration during O$_2$ purging on the degradation of Bentazon by UV/ZnO/TiO$_2$ process was investigated at initial pH 7, catalyst dosage (0.5 g/L), initial concentration of Bentazon (20 ppm), and gas flow rate was 2 L/min for different time interval. Fig. 9 shows the effect of purging of oxygen gas and variation of DO concentration. As shown in Fig. 9, photocatalytic degradation of Bentazon was enhanced with purging of oxygen gas when compared to that without purging of oxygen gas. The degradation efficiency with purging of oxygen gas increased from 44.4 to 99.9% by increasing time from 15 to 120 min, while it was ranged from 30.1 to 84.2% without purging of oxygen gas. As exhibited in Fig. 8, the DO concentration decreased from 19.5 to 9.9 ppm by increasing time from 15 to 120 min. In the purging of oxygen gas, electron scavenging can be increased. Electrons generated in conduction band are effectively consumed by increased dissolved oxygen and inhibit recombination between positive hole and electron [41].
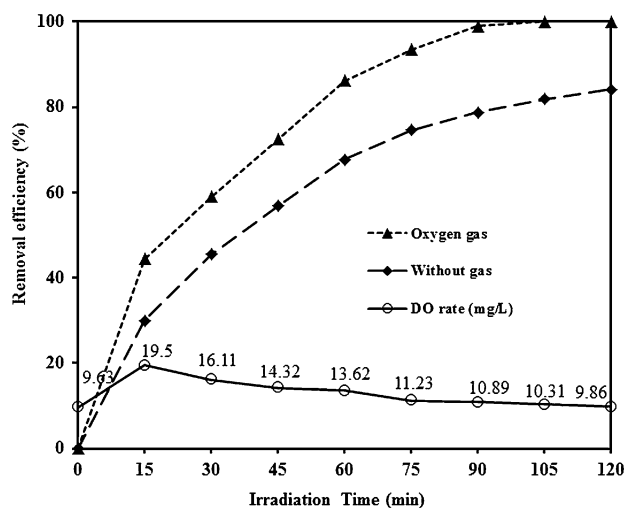

Fig. 9. The effect of purging of oxygen gas and variation of DO concentration during O$_2$ purging on the photocatalytic degradation of Bentazon (catalyst dosage = 0.5 g/L, pH 7, [Bentazon]$_0$ = 20 ppm).

3.2.6. Effect of the hydrogen peroxide

Effect of the initial hydrogen peroxide concentration (2, 5, 10, 25, 50 mM) on the photocatalytic degradation of Bentazon by UV/ZnO/TiO$_2$ process was investigated at initial pH 7, catalyst dosage (0.5 g/L), and initial concentration of Bentazon (20 ppm) for different time intervals. Fig. 10 shows the effect of the hydrogen peroxide concentration on photocatalytic degradation of Bentazon. Fig. 10 shows the degradation efficiency enhanced from 86.3 to 99.9% by increasing the initial hydrogen peroxide concentration from 2 to 10 mM. The increased photocatalytic degradation efficiency of Bentazon after the addition of hydrogen peroxide can be explained by the increased reaction between hydrogen peroxide and electron in the conduction band of Bentazon. According to Eq. (10), hydrogen peroxide can effectively inhibit the electron–hole recombination. Since hydrogen peroxide is a better electron acceptor than dissolved oxygen, it could act as an alternative electron acceptor to oxygen [37]. At low concentration of hydrogen peroxide, inhibition of the electron–hole recombination is effectively contributed to the photocatalytic degradation of Bentazon. However, further increase in hydrogen peroxide concentration above 10 mM caused lower degradation of Bentazon due to an inhibitive effect on the reaction between Bentazon and electron in the conduction band of ZnO/TiO$_2$
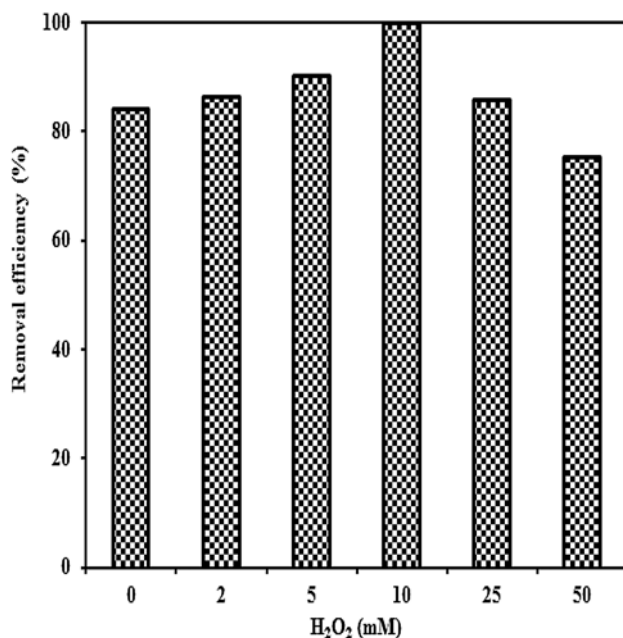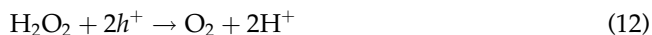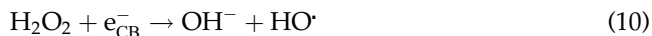

Fig. 10. The effect of hydrogen peroxide on the photocatalytic degradation of Bentazon (catalyst dosage = 0.5 g/L, pH 7, [Bentazon]$_0$ = 20 ppm).

nanocomposite (Eq. 11) [21]. The other reason for the inhibition effect can also be explained in terms of scavenging of positive holes by adsorbed H$_2$O$_2$ on the surface of ZnO/TiO$_2$ nanocomposite (Eq. 12) [21,42].

$$H_2O_2 + e_{CB}^- \rightarrow OH^- + HO^{\cdot} \tag{10}$$

$$H_2O_2 + OH^{\cdot} \rightarrow HO_2^{\cdot} + H_2O \tag{11}$$

$$H_2O_2 + 2h^+ \rightarrow O_2 + 2H^+ \tag{12}$$

3.2.7. Effect of the organic compounds

Effect of the presence of different types of organic compounds such as (humic acid, oxalate acid, EDTA, phenol, folic acid, citric acid) (20 ppm) on the photocatalytic degradation of Bentazon by UV/ZnO/TiO$_2$ process was investigated at initial pH 7, catalyst dosage (0.5 g/L), and initial concentration of Bentazon (20 ppm) for different time intervals. As shown in Fig. 11, any type of organic compounds showed inhibition effect on the photocatalytic degradation of Bentazon. One role of added organic compound is blocking of active sites on the photocatalysts by competitive adsorption. The other role of added organic compound is decreasing of electron–hole recombination due to scavenging of positive holes in valence band by organic compounds. Considering the observed results, second role was not greater than the first role [43–45].

3.2.8. The comparison of each process

To evaluate the effect of various processes involved in the photocatalytic degradation of Bentazon, removal of Bentazon by ZnO-alone, UV-alone, ZnO/TiO$_2$ alone, TiO$_2$-alone, UV/ZnO, UV/TiO$_2$, and UV/ZnO/TiO$_2$ process was evaluated at pH 7, photocatalyst dosage of 0.5 g/L, and 20 ppm Bentazon concentration (Fig. 12). The result showed that the removal efficiency by each process was 0.9, 3.4, 4.4, 5.47, 33.3, 64.9, and 84.2%. The photocatalytic degradation of Bentazon through just adsorption process was insignificant. As can be seen from Fig. 12, the photocatalytic degradation efficiency of Bentazon by UV/ZnO/TiO$_2$ process was about 84.2%, which was greater than that by UV/TiO$_2$ (64.9%) and UV/ZnO (33.3%) processes. In agreement with our study, Mir et al. reported removal efficiency of Bentazon by UVC-125 W-alone was 9.5% [21]. Near complete removal of Bentazon by UV/ZnO–TiO$_2$/H$_2$O$_2$ and
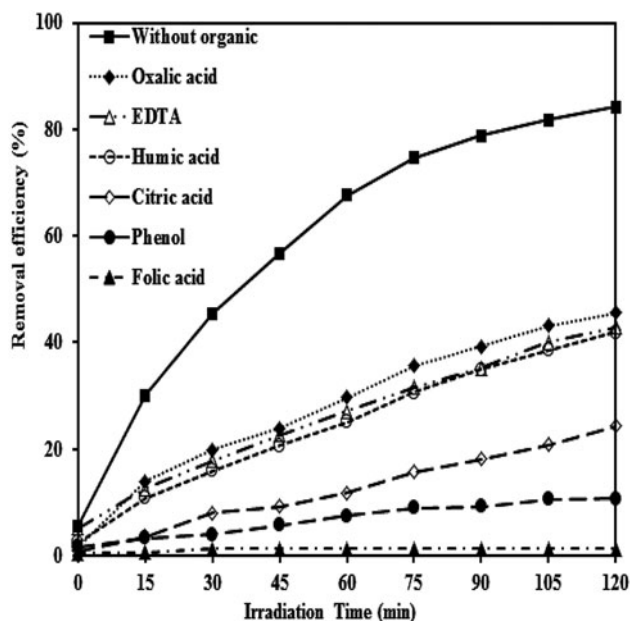
Fig. 11. The effect of different organic compounds on the photocatalytic degradation of Bentazon (catalyst dosage = 0.5 g/L, pH 7, [Bentazon]$_0$ = 20 ppm, organic compounds = 20 ppm).
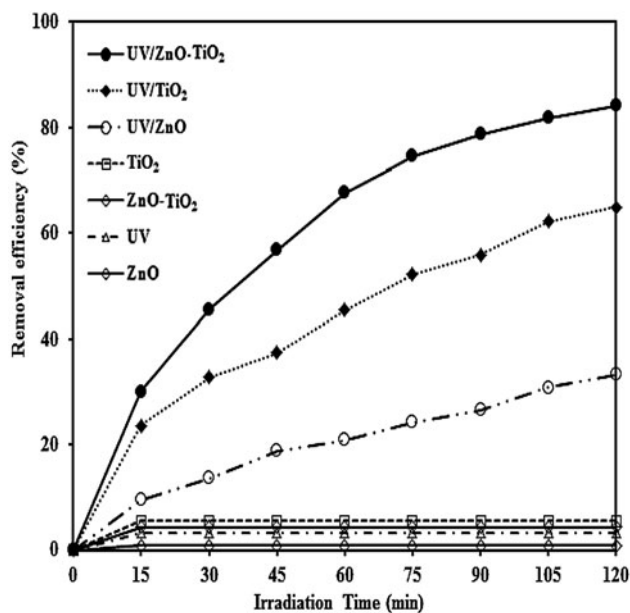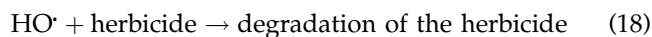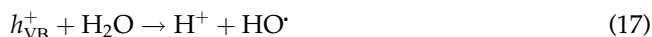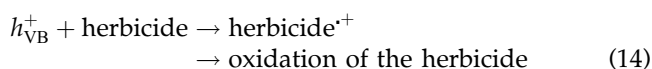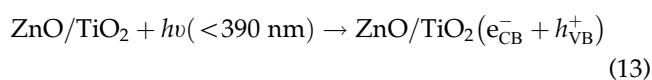

Fig. 12. The contribution of each process involved in the photocatalytic degradation of Bentazon (catalyst dosage = 0.5 g/L, pH 7, [Bentazon]$_0$ = 20 ppm).

UV/ZnO–TiO$_2$/O$_2$ was reported. This comparison shows that the ZnO/TiO$_2$ composite is an effective catalyst for the photocatalytic degradation of Bentazon

from aqueous solution compared to ZnO-alone or TiO$_2$-alone. The plausible reason for the enhanced removal of Bentazon by ZnO/TiO$_2$ nanocomposites may be due to an electron transfer from the conduction band of ZnO to the conduction band of TiO$_2$ as well as a hole transfer from the valence band of TiO$_2$ to the valance band of ZnO. This efficient charge separation can increase the lifetime of the charge carriers and enhance the photocatalytic efficiency of ZnO/TiO$_2$ composites compared to ZnO-alone or TiO$_2$-alone [14,19,46]. Based on the above experiments and analysis, mechanism of the photocatalysis could be proposed as the following reactions [3,7,8]:

$$ZnO/TiO_2 + h\upsilon(<390\ nm) \rightarrow ZnO/TiO_2\left(e_{CB}^- + h_{VB}^+\right)$$
(13)

$$h_{VB}^+ + herbicide \rightarrow herbicide^{\cdot+}$$
$$\rightarrow oxidation\ of\ the\ herbicide \quad (14)$$

$$h_{VB}^+ + H_2O \rightarrow H^+ + HO^\cdot \qquad (15)$$

$$h_{VB}^+ + OH^- \rightarrow HO \qquad (16)$$

$$h_{VB}^+ + H_2O \rightarrow H^+ + HO^\cdot \qquad (17)$$

$$HO^\cdot + herbicide \rightarrow degradation\ of\ the\ herbicide \quad (18)$$

The temporal distribution of species of the decomposition of Bentazon in aqueous solution by advance oxidation process was reported by authors. Possible route for the photocatalytic degradation of Bentazone in the presence of TiO$_2$ was reported by Seck et al. [8]. It was found that the hydroxylation of isopropyl group in bentazone is the main pathway, and then formation of sulfate ions was stoichiometrically detected and was accomplished at a very early period of the decomposition of Bentazon, and then the formation of the nitrate ions was to be proceeded. Finally nitrate ions conversion indicating the mineralization of one atom of the organic nitrogen of the Bentazon. These findings can be explained by observing the structure of Bentazon. Similar results and the complete decomposition pathways of Bentazon in aqueous solutions by advance oxidation process have been reported by Mir et al. [21].

The ability of a photocatalyst for continuous removal of organic contaminants is a significant criterion. Hence, the photocatalytic degradation of Bentazon was performed by ZnO/TiO$_2$ nanocomposite for five repeated runs. As can be seen in Fig. 13, the synthesized photocatalyst showed quite similar photocatalytic activity even after five repeated runs.
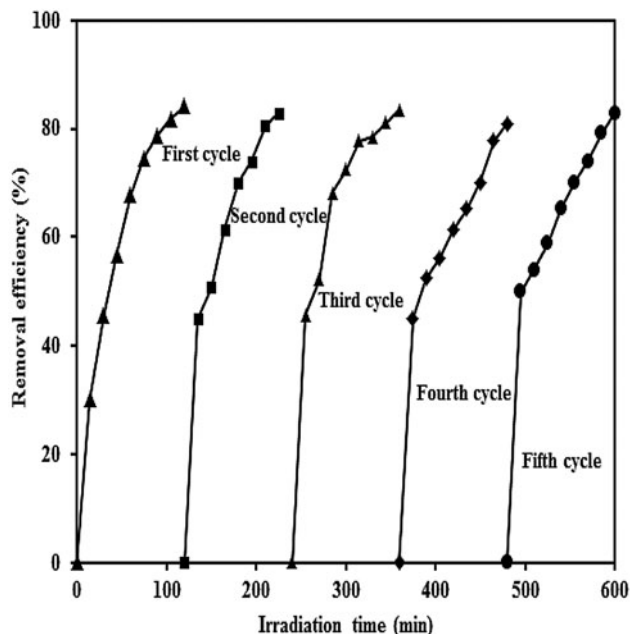
Fig. 13. Reusability test for the photocatalytic degradation of Bentazon within five repeated cycles (catalyst dosage = 0.5 g/L, pH 7, $[Bentazon]_0$ = 20 ppm).

4. Conclusion

In the present research, the application of ZnO/TiO_2 nanocomposites for photocatalytic degradation of Bentazon in aqueous solutions was studied. The prepared sample was characterized by of SEM, EDX, XRD, and FT-IR. The results indicated more photocatalytic activity of the ZnO/TiO_2 nanocomposite in comparison with any processes. As the nanocatalyst dosage increased, the photocatalytic degradation of the Bentazon was continuously enhanced, but was gradually decreased above 0.5 g/L. Maximum degradation efficiency was observed at neutral pH because the reduced photocatalytic activity of nanocatalyst at exceedingly low and high pH values originates from photo-corrosion of ZnO. By first-order kinetic assumption, the values of the kinetic rate and the L–H adsorption constants were determined as 0.1621 L/mg and 0.154 mg/L/min, respectively. The electrical energy consumption per order of magnitude for photocatalytic degradation of Bentazon by $UV/ZnO/TiO_2$ process was lower than that by UV/TiO_2, UV/ZnO, and UV process, which confirmed the better performance of ZnO/TiO_2 composite due to an enhanced charge separation. The removal efficiency of Bentazon increased with purging of oxygen gas and hydrogen peroxide (up to 10 mM) compared to that of without them. Organic compounds showed inhibition effect on the degradation of Bentazon.

References

[1] N. Daneshvar, D. Salari, A. Niaei, A.R. Khataee, Photocatalytic degradation of the herbicide erioglaucine in the presence of nanosized titanium dioxide: Comparison and modeling of reaction kinetics, J. Environ. Sci. Health Part A Toxic/Hazard. Subst. Environ. Eng. 41 (2006) 1273–1290.

[2] E. Ayranci, N. Hoda, Adsorption of bentazon and propanil from aqueous solutions at the high area activated carbon-cloth, Chemosphere 57 (2004) 755–762.

[3] B. Eyheraguibel, A. Ter Halle, C. Richard, Photodegradation of bentazon, clopyralid, and triclopyr on model leaves: Importance of a systematic evaluation of pesticide photostability on crops, J. Agric. Food. Chem. 57 (2009) 1960–1966.

[4] R. Pourata, A. Khataee, S. Aber, N. Daneshvar, Removal of the herbicide Bentazon from contaminated water in the presence of synthesized nanocrystalline TiO_2 powders under irradiation of UV-C light, Desalination 249 (2009) 301–307.

[5] J. Salman, V. Njoku, B. Hameed, Bentazon and carbofuran adsorption onto date seed activated carbon: Kinetics and equilibrium, Chem. Eng. J. 173 (2011) 361–368.

[6] World Health Organisation (WHO), WHO Guidelines for Drinking Water Quality, World Health Organisation, Geneva, 2004, p. 311.

[7] M. Davezza, D. Fabbri, E. Pramauro, A. Bianco Prevot, Photocatalytic degradation of bentazone in soil washing wastes containing alkylpolyoxyethylene surfactants, Chemosphere 86 (2012) 335–340.

[8] E. Seck, J. Doña-Rodríguez, C. Fernández-Rodríguez, O. González-Díaz, J. Araña, J. Pérez-Peña, Photocatalytical removal of bentazon using commercial and sol–gel synthesized nanocrystalline TiO_2: Operational parameters optimization and toxicity studies, Chem. Eng. J. 203 (2012) 52–62.

[9] N.M. Mahmoodi, M. Arami, N.Y. Limaee, K. Gharanjig, F.D. Ardejani, Decolorization and mineralization of textile dyes at solution bulk by heterogeneous nanophotocatalysis using immobilized nanoparticles of titanium dioxide, Colloids Surf., A. 290 (2006) 125–131.

[10] P. Niu, J. Hao, Photocatalytic degradation of methyl orange by titanium dioxide-decatungstate nanocomposite films supported on glass slides, Colloids Surf., A. 431 (2013) 127–132.

[11] U. Akpan, B. Hameed, Photocatalytic degradation of 2, 4-dichlorophenoxyacetic acid by $Ca–Ce–W–TiO_2$ composite photocatalyst, Chem. Eng. J. 173 (2011) 369–375.

[12] M. Farrokhi, J.-K. Yang, S.-M. Lee, M. Shirzad-Siboni, Effect of organic matter on cyanide removal by illuminated titanium dioxide or zinc oxide nanoparticles, Iran. J. Environ. Health Sci. Eng. 11 (2013) 23.

[13] T. Kawano, H. Imai, A simple preparation technique for shape-controlled zinc oxide nanorods: Formation of narrow size-distributed nanorods using seeds in aqueous solutions, Colloids Surf., A. 319 (2008) 130–135.

[14] M. Naimi-Joubani, M. Shirzad-Siboni, J.-K. Yang, M. Gholami, M. Farzadkia, Photocatalytic reduction of hexavalent chromium with illuminated ZnO/TiO₂ composite, J. Ind. Eng. Eng. Chem. 22 (2015) 317–323.

[15] Y. Tang, G. Zhang, C. Liu, S. Luo, X. Xu, L. Chen, B. Wang, Magnetic TiO₂-graphene composite as a high-performance and recyclable platform for efficient photocatalytic removal of herbicides from water, J. Hazard. Mater. 252–253 (2013) 115–122.

[16] I. Losito, A. Amorisco, F. Palmisano, P. Zambonin, X-ray photoelectron spectroscopy characterization of composite TiO₂–poly(vinylidenefluoride) films synthesised for applications in pesticide photocatalytic degradation, Appl. Surf. Sci. 240 (2005) 180–188.

[17] F.C. Doria, A. Borges, J. Kim, A. Nathan, J. Joo, L. Campos, Removal of metaldehyde through photocatalytic reactions using nano-sized zinc oxide composites, Water Air Soil Pollut. 224 (2013) 1–9.

[18] Z.-P. Yang, X.-Y. Gong, C.-J. Zhang, Recyclable Fe₃O₄/hydroxyapatite composite nanoparticles for photocatalytic applications, Chem. Eng. J. 165 (2010) 117–121.

[19] Y. Xiaodan, W. Qingyin, J. Shicheng, G. Yihang, Nanoscale ZnS/TiO₂ composites: Preparation, characterization, and visible-light photocatalytic activity, Mater. Charact. 57 (2006) 333–341.

[20] M.V.P. Sharma, V. Durgakumari, M. Subrahmanyam, Solar photocatalytic degradation of isoproturon over TiO₂/H-MOR composite systems, J. Hazard. Mater. 160 (2008) 568–575.

[21] N.A. Mir, M. Haque, A. Khan, M. Muneer, S. Vijayalakshmi, Photocatalytic degradation of herbicide Bentazone in aqueous suspension of TiO₂: Mineralization, identification of intermediates and reaction pathways, Environ. Technol. 35 (2014) 407–415.

[22] J.M. Salman, K. Al-Saad, Batch study for herbicide bentazon adsorption onto palm oil fronds activated carbon, Int. J. Chem. Sci. 10 (2012) 731–740.

[23] M. Shirzad Siboni, M.T. Samadi, J.K. Yang, S.M. Lee, Photocatalytic reduction of Cr(VI) and Ni(II) in aqueous solution by synthesized nanoparticle ZnO under ultraviolet light irradiation: A kinetic study, Environ. Technol. 32 (2011) 1573–1579.

[24] M. Shirzad-Siboni, S.J. Jafari, O. Giahi, I. Kim, S.-M. Lee, J.-K. Yang, Removal of acid blue 113 and reactive black 5 dye from aqueous solutions by activated red mud, J. Ind. Eng. Chem. 20 (2014) 1432–1437.

[25] M. Shirzad-Siboni, A. Khataee, S.W. Joo, Kinetics and equilibrium studies of removal of an azo dye from aqueous solution by adsorption onto scallop, J. Ind. Eng. Chem. 20 (2014) 610–615.

[26] M. Shirzad-Siboni, A. Khataee, F. Vafaei, S.W. Joo, Comparative removal of two textile dyes from aqueous solution by adsorption onto marine-source waste shell: Kinetic and isotherm studies, Korean J. Chem. Eng. (2014) 1–9.

[27] M. Farrokhi, S.-C. Hosseini, J.-K. Yang, M. Shirzad-Siboni, Application of ZnO–Fe₃O₄ nanocomposite on the removal of azo dye from aqueous solutions:

[28] W. Horwitz (Ed.), Standard Methods for the Examination of Water and Wastewater, twenty ed., APHA, Washington, DC, 2000.

[29] K.S. Babu, V. Narayanan, Hydrothermal synthesis of hydrated zinc oxide nanoparticles and its Characterization, Chem. Sci. Trans. 2(S1) (2013) S33–S36.

[30] M. Grujic-Brojcin, M. Scepanovic, Z. Dohcevic-Mitrovic, Z. Popovic, Infrared study of nonstoichiometric anatase TiO2 nanopowders, Sci. Sintering 38 (2006) 183–189.

[31] N. Daneshvar, S. Aber, M.S. Seyeddorraji, A.R. Khataee, M.H. Rasoulifard, Photocatalytic degradation of the insecticide diazinon in the presence of prepared nanocrystalline ZnO powders under irradiation of UV-C light, Sep. Purif. Technol. 58 (2007) 91–98.

[32] S. Devipriya, S. Yesodharan, Photocatalytic degradation of pesticide contaminants in water, Sol. Energy Mater. Sol. Cells 86 (2005) 309–348.

[33] A. Nezamzadeh-Ejhieh, S. Khorsandi, Photocatalytic degradation of 4-nitrophenol with ZnO supported nano-clinoptilolite zeolite, J. Ind. Eng. Chem. 20 (2014) 937–946.

[34] S. Rabindranathan, S. Devipriya, S. Yesodharan, Photocatalytic degradation of phosphamidon on semiconductor oxides, J. Hazard. Mater. 102 (2003) 217–229.

[35] P. Wongkalasin, S. Chavadej, T. Sreethawong, Photocatalytic degradation of mixed azo dyes in aqueous wastewater using mesoporous-assembled TiO₂ nanocrystal synthesized by a modified sol–gel process, Colloids Surf., A. 384 (2011) 519–528.

[36] S. Xu, J. Ng, X. Zhang, H. Bai, D.D. Sun, Adsorption and photocatalytic degradation of Acid Orange 7 over hydrothermally synthesized mesoporous TiO₂ nanotube, Colloids Surf., A. 379 (2011) 169–175.

[37] N. Daneshvar, M.H. Rasoulifard, A.R. Khataee, F. Hosseinzadeh, Removal of C.I. Acid Orange 7 from aqueous solution by UV irradiation in the presence of ZnO nanopowder, J. Hazard. Mater. 143 (2007) 95–101.

[38] M. Shirzad Siboni, M.-T. Samadi, J.-K. Yang, S.-M. Lee, Photocatalytic removal of Cr(VI) and Ni(II) by UV/TiO₂: Kinetic study, Desalin. Water Treat. 40 (2012) 77–83.

[39] M. Shirzad-Siboni, M. Farrokhi, R. Darvishi Cheshmeh Soltani, A. Khataee, S. Tajassosi, Photocatalytic reduction of hexavalent chromium over zno nanorods immobilized on kaolin, Ind. Eng. Chem. Res. 53 (2014) 1079–1087.

[40] M. Shirzad-Siboni, M. Samarghandi, J.-K. Yang, S.-M. Lee, Photocatalytic removal of reactive Black-5 Dye from aqueous solution by UV irradiation in aqueous TiO₂: Equilibrium and kinetics study, J. Adv. Oxid. Technol. 14 (2011) 302–307.

[41] T. Zhang, T. Oyama, A. Aoshima, H. Hidaka, J. Zhao, N. Serpone, Photooxidative N-demethylation of methylene blue in aqueous TiO₂ dispersions under UV irradiation, J. Photochem. Photobiol., A. 140 (2001) 163–172.

[42] N. Daneshvar, D. Salari, A.R. Khataee, Photocatalytic degradation of azo dye acid red 14 in water: Investigation of the effect of operational parameters, J. Photochem. Photobiol., A. 157 (2003) 111–116.

Kinetics and equilibrium studies, Water Air Soil Pollut. 225 (2014) 1–12.

[43] J.K. Yang, S.M. Lee, M. Farrokhi, O. Giahi, M. Shirzad Siboni, Photocatalytic removal of Cr(VI) with illuminated TiO$_2$, Desalin. Water Treat. 46 (2012) 375–380.

[44] J.K. Yang, S.M. Lee, M. Siboni, Effect of different types of organic compounds on the photocatalytic reduction of Cr(VI), Environ. Technol. 33 (2012) 2027–2032.

[45] M.R. Samarghandi, J.K. Yang, S.M. Lee, O. Giahi, M. Shirzad-Siboni, Effect of different type of organic compounds on the photocatalytic reduction of Cr(VI) in presence of ZnO nanoparticles, Desalin. Water Treat. 52 (2013) 1–8.

[46] Y. Cai, H. Fan, M. Xu, Q. Li, Rapid photocatalytic activity and honeycomb Ag/ZnO heterostructures via solution combustion synthesis, Colloids Surf., A. 436 (2013) 787–795.